nature geoscience

ARTICLES

https://doi.org/10.1038/s41561-018-0186-5

Holocene dynamics of the Southern Hemisphere westerly winds and possible links to CO_2 outgassing

Krystyna M. Saunders[1,2*], Stephen J. Roberts[3], Bianca Perren[3], Christoph Butz[1], Louise Sime[3], Sarah Davies[4], Wim Van Nieuwenhuyze[5], Martin Grosjean[1] and Dominic A. Hodgson[3,6]

The Southern Hemisphere westerly winds (SHW) play an important role in regulating the capacity of the Southern Ocean carbon sink. They modulate upwelling of carbon-rich deep water and, with sea ice, determine the ocean surface area available for air–sea gas exchange. Some models indicate that the current strengthening and poleward shift of these winds will weaken the carbon sink. If correct, centennial- to millennial-scale reconstructions of the SHW intensity should be linked with past changes in atmospheric CO_2, temperature and sea ice. Here we present a 12,300-year reconstruction of wind strength based on three independent proxies that track inputs of sea-salt aerosols and minerogenic particles accumulating in lake sediments on sub-Antarctic Macquarie Island. Between about 12.1 thousand years ago (ka) and 11.2 ka, and since about 7 ka, the wind intensities were above their long-term mean and corresponded with increasing atmospheric CO_2. Conversely, from about 11.2 to 7.2 ka, the wind intensities were below their long-term mean and corresponded with decreasing atmospheric CO_2. These observations are consistent with model inferences of enhanced SHW contributing to the long-term outgassing of CO_2 from the Southern Ocean.

The Southern Ocean currently accounts for $43 \pm 3\%$ of the global oceanic anthropogenic CO_2 uptake[1] mitigating (perhaps temporarily) the climatic effects of enhanced greenhouse gases in the atmosphere. The capacity of the Southern Ocean to absorb CO_2 at the surface is determined by the balance between processes sequestering carbon (such as diffusion and the biological carbon pump) and processes releasing old carbon from the deep ocean to the atmosphere (such as upwelling and outgassing)[2,3]. Attempts to model these processes have yielded conflicting results. One model based on instrumental data collected between 1981 and 2004 suggested that the Southern Ocean carbon sink has weakened[4]. Conversely, analyses of the same data extended to 2011 suggest a reinvigoration of the carbon sink since 2002[5]. This latter trend is also seen in measurements of the difference between the partial pressure of CO_2 in ocean surface water and the overlying atmosphere (Δp_{CO_2}) of the Southern Ocean in Drake Passage[6]. Spatial extrapolation of the relatively few p_{CO_2} measurements from the Southern Ocean as a whole suggests a trend towards a weakening sink in the 1990s but a strengthening one in the 2000s[7].

The SHW, which are strongest from 50° S to 55° S over the Southern Ocean[8] (Fig. 1a), are one of the main drivers of the Southern Ocean CO_2 sink. Changes in the SHW are mainly determined by atmospheric temperature gradients, sea surface temperature and regional sea ice[9]. In turn, they influence ocean circulation[10,11], regulate sea ice extent[12] and control the upwelling of deep water rich in dissolved inorganic carbon to Antarctic surface waters[2]. All are processes that modulate the net uptake of CO_2 by the ocean from the atmosphere[13]. Studies that propose a weakening of the Southern Ocean CO_2 sink attribute it to the recent strengthening and poleward shift of the SHW resulting from changes in surface temperature gradients due to human activities, including ozone depletion[4]. This has brought carbon-rich waters to the surface ocean and reduced Δp_{CO_2} (ref. [1]).

Despite the potential importance of the SHW in modulating net uptake of CO_2 by the Southern Ocean, recent extrapolations of the future behaviour of the CO_2 sink are solely based on short-term instrumental records and sparse measurements of Δp_{CO_2} (refs [4,5]). If current theories regarding a potential weakening of the CO_2 sink are correct, past reconstructions of changes in the intensity of the SHW over the Southern Ocean should show clear links between atmospheric CO_2, temperature and sea ice over longer (centennial to millennial) timescales.

So far, palaeoclimatic reconstructions of the SHW derive mostly from southernmost South America, the only continental landmass intersecting the mid to northern core of the SHW. However, they "do not provide a consistent picture of the SHW during the Holocene" (ref. [14], p.14). This can be partly attributed to a reliance on proxies of past changes in effective precipitation and/or temperature to infer changes in wind strength. Examples include subfossil pollen assemblages in peat and lake sediment cores (for example refs [15,16]), geochemical proxies of the precipitation–evaporation balance (for example ref. [17]), and rainfall changes influencing runoff into fjord[18] and ocean[19] sediments. The application of proxies (such as exotic pollen[20,21] or dust[22]) that measure wind-blown transport is rare, and their relationship to wind strength not always straightforward[14].

Avoiding continental landmasses with complex orographic effects, and applying multi-proxy (and independent) methods to track past changes in wind intensity, circumvents these issues. The latter tests whether different wind proxies record congruent patterns in the direction and relative magnitude of change, providing a validation that the proxies are responding to the external forcing of the SHW, rather than local or internal dynamics at the study site.

We carried out a detailed reconstruction of Holocene changes in SHW intensity at sub-Antarctic Macquarie Island. The first aim was to reconstruct changes in the dynamics and relative strength of

[1]Institute of Geography and Oeschger Centre for Climate Change Research, University of Bern, Bern, Switzerland. [2]Australian Nuclear Science and Technology Organisation, Sydney, Australia. [3]British Antarctic Survey, Cambridge, UK. [4]Department of Geography and Earth Sciences, Aberystwyth University, Aberystwyth, UK. [5]Department of Biology, University of Ghent, Ghent, Belgium. [6]Department of Geography, University of Durham, Durham, UK. *e-mail: krystyna.saunders@ansto.gov.au

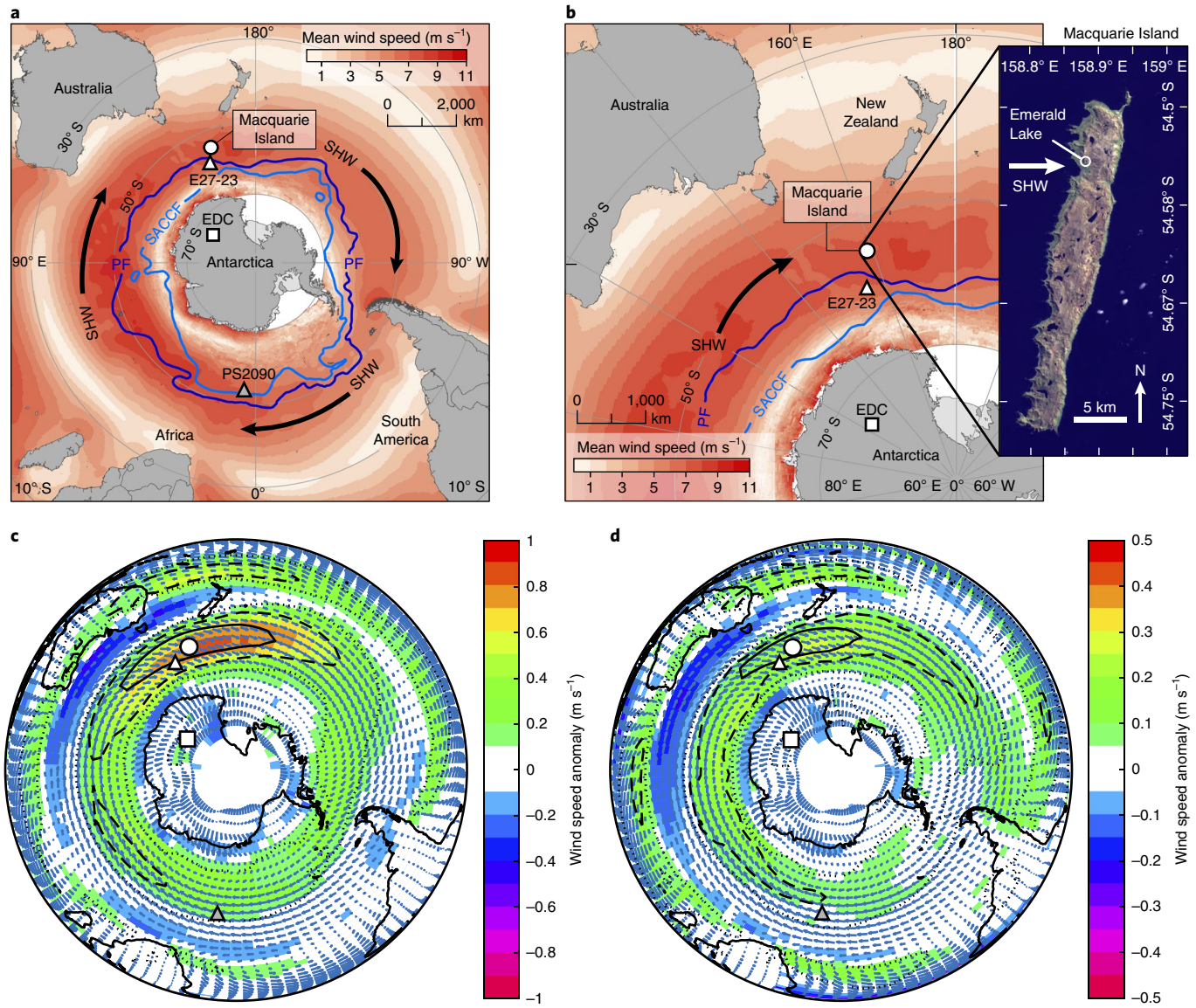

Fig. 1 | SHW and wind anomalies in relation to the location of Macquarie Island a, Location of Macquarie Island (white circle) in the Southern Ocean within the core of the SHW belt. White square, EPICA Dome C ice core (EDC); grey triangle, marine core PS2090; white triangle, marine core E27-23; PF, Polar Front, SACCF, Southern Antarctic Circumpolar Current Front. **b**, Location of Macquarie Island and Emerald Lake (pan-sharpened Landsat8 satellite image, bands 4, 3, 2). **c**,**d**, Annual mean (**c**) and decadal (**d**) wind speed anomalies associated with the top 20% of highest wind speed events at Macquarie Island, based on a 400 year pre-industrial simulation using the HadCM3 model. Dashed (and solid) black contours show the 0.5 (and 0.75) correlations associated between Macquarie Island wind changes and changes in wind elsewhere in the Southern Hemisphere (see Supplementary Notes 1 and 2 for details).

the SHW over the core jets of the Antarctic Circumpolar Current, the region most relevant to air–sea gas exchange in the Southern Ocean[23]. The second was to test which of the competing models of a weakening[4] or reinvigoration[5] of the carbon sink in recent decades is supported by the long-term palaeo-record. We did not consider changes in the position of the SHW core belt (50°–55° S) in detail. More multi-proxy, well-dated, records are needed from broader latitudinal and longitudinal ranges to reliably separate changes in intensity from changes in latitudinal position.

Sub-Antarctic Macquarie Island

Macquarie Island is a small (130 km^2) island located a few hundred kilometres north of the Polar Front (54° S, 158° E; Fig. 1 and Supplementary Note 1). The sub-Antarctic islands are the only landmasses, other than southernmost South America, that lie in the core of the SHWs. Macquarie Island experiences mean annual wind speeds of about 35 km h^{-1}, a mean daily wind run of 751 km and gusts of up to 185 km h^{-1} (ref. [24]), and its climate is representative of the core belt of the SHW (Fig. 1c,d). Wind almost exclusively comes from the west-northwest (Supplementary Figs. 2 and 3). This results in strong west-to-east gradients in sea spray[25] and minerogenic wind-blown aerosols being deposited across the island. These aerosols accumulate over time in lake and peat sediments, preserving a record of relative changes in SHW intensity, with periods of more (or less) sea spray or deposited minerogenic material reflecting phases of stronger (or weaker) winds. We applied a combination of three methods to reconstruct past changes in SHW intensity using a sedimentary sequence from Emerald Lake, a small lake perched on the western edge of the Macquarie Island plateau that is directly exposed to westerly air flow (Supplementary Note 2). The sediment

sequence was radiometrically dated with 44 ^{14}C and 11 ^{210}Pb dates (Supplementary Note 3). Inference models based on diatoms provided a measure of past inputs of sea spray aerosols through their effect on the conductivity and diatom species assemblages in lakes[25]. These were compared with two independent measures of minerogenic aerosol inputs based on micro-X-ray fluorescence (μ-XRF) core scanning and hyperspectral imaging. These proxies, and the sedimentology of the core, are described in Supplementary Notes 4, 5.

Holocene dynamics of the SHW

The three proxies used in the present study show similar patterns in wind strength over Macquarie Island over the past ~12.3 kyr (Fig. 2; Supplementary Note 5). The strongest correlation is between the two methods measuring minerogenic inputs (correlation coefficient $r=0.85$, $P<0.0001$, Supplementary Table 4). These are also significantly correlated with the independent diatom-inferred conductivity/sea-spray proxy ($r=0.56$ and $r=0.65$, $P<0.0001$). The slightly weaker correlations with the diatom-inferred conductivity/sea-spray proxy can be attributed to lake water nutrients and pH, which explain smaller yet independent portions of the variance in the diatom data[25]. The correlations between the minerogenic wind proxies and diatom-inferred conductivity exclude changes in dust supply from source regions as a major factor modifying the reconstructions. The period from 7.5 to 7.2 ka shows a negative correlation between the minerogenic proxies and diatom-inferred conductivity. Based on the presence of sub-aerial diatoms, this was attributed to a brief period of low water levels (see Supplementary Note 4).

In general, the proxies show high relative wind intensity (defined here as periods when at least two of the three wind proxies have values greater than the 95% upper bound of their mean; Supplementary Table 6) in the periods 12.1–11.2, 9.2–8.5, 7.9–7.7, 7.0–5.6, 5.3–0.2 and 0.1–0 ka. Low relative wind intensities were recorded for 11.2–9.2, 8.4–7.9, 7.7–7.0 and 0.2–0.1 ka. The key features are high relative winds spanning the end of the Last Glacial–Interglacial Transition (LGIT) to the early Holocene (12.1–11.2 ka), low relative winds during the early Holocene Thermal Maximum (11.2–9.2 ka), increased winds and higher-amplitude changes for 9.2–5.3 ka, and a period of sustained relatively intense winds from 5.3 to 0.2 ka (although the resolution of the record is lower during this period) (Fig. 2). After 0.2 ka, the wind intensity drops, and then it increases in the most recent decades.

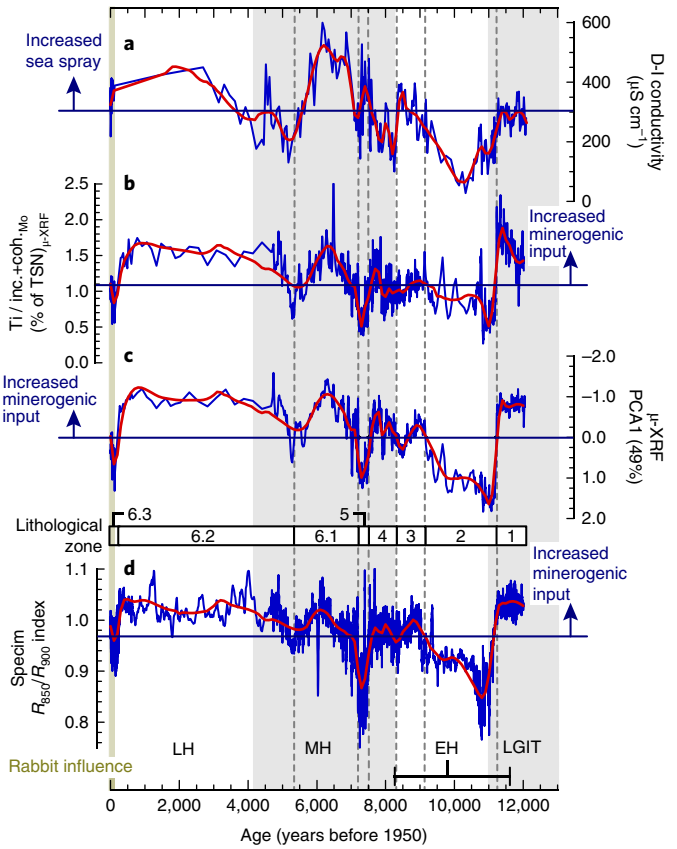

Fig. 2 | Changes in relative strength of the Southern Hemisphere westerly winds based on proxies in a sediment core from Emerald Lake. **a**, Diatom-inferred (D-I) conductivity. **b**, Titanium μ-XRF analysis. **c**, Micro-XRF principal components analysis (PCA), axis 1. **d**, Hyperspectral ratio (R_{850}/R_{900}). Red lines indicate 100-year interval second-order LOESS-smoothing. Periods of increased wind strength are defined as greater than the 95% upper bound of the mean (dark blue horizontal lines; see Supplementary Note 5 and Supplementary Table 6). Khaki shading (Rabbit influence) indicates when proxies were compromised by erosional inputs from non-indigenous species[42]. LGIT, Last Glacial–Interglacial Transition (grey shading); EH, early Holocene; MH, mid Holocene (grey shading); LH, late Holocene. Horizontal bar labelled EH indicates formal early Holocene. Grey dashed lines are lithological zones; lithology is described in Supplementary Table 3 and Note 4. TSN, total scatter normalized; Ti, titanium; inc., incoherent (or Compton scattering); coh., coherent (or Rayleigh scattering); Mo., molybdenum tube (see Supplementary Note 4).

SHW dynamics, atmospheric CO_2, sea ice and temperature

Significant correlations between the three independent wind proxies support the hypothesis that, together, they provide a reliable record of changes in the dynamics of the SHW in their core belt, and more specifically at Macquarie Island. Therefore, to address our wider objective of evaluating the role of the SHW as a driver of natural CO_2 variations, we compared past changes in the SHW at Macquarie Island with other hemispheric changes in the ocean and atmosphere. These include far-field proxy records in the EPICA Dome C core of sea ice (sea-salt Na^+ aerosol flux, ssNa)[26], temperature and CO_2 (ref. [2]), and winter sea-ice concentration (WSIC) based on microfossil measurements in selected (and not necessarily representative) marine cores from the South Atlantic (PS2090[27]) and South Pacific sector near Macquarie Island (E27-23[28]; Fig. 3).

12.1–11.2 ka. The end of the LGIT and early Holocene are characterized by intense SHW. Many records at similar latitudes in southernmost South America (Supplementary Fig. 15c–e) and elsewhere in the Southern Hemisphere (Supplementary Note 7) agree. This period of intense SHW is accompanied by marked increases in atmospheric CO_2 and temperature (Fig. 3e,f), and declines in sea ice (Fig. 3c,d). There are both proxy and model-based studies that support the magnitude and direction of these changes across the LGIT[10,29,30]. Specifically, the persistent winds identified here are consistent with enhanced Southern Ocean upwelling[10] accounting for at least part of the deglacial rise in atmospheric CO_2, and accompanied by increases in atmospheric[30] and sea surface temperatures[29]. Temporal patterns in our records are also consistent with the retreat of sea ice having a positive feedback on the ocean surface area available for the outgassing of CO_2 (ref. [29]; Fig. 3).

11.2–9.2 ka. An early Holocene thermal maximum between 11.2 and 9.2 ka is clearly resolved in Antarctica[31] and other records across the Southern Hemisphere, including the western side of the Andes from 49° to 55° S (ref. [14]). This reduced the thermal gradient between the mid and high latitudes and resulted in persistent low-intensity winds at Macquarie Island (Fig. 3a,b). This is consistent with selected records from South America[32,33], Tasmania and New Zealand[32] (Supplementary Note 7), and a reduced thermal gradient in the Southern Ocean

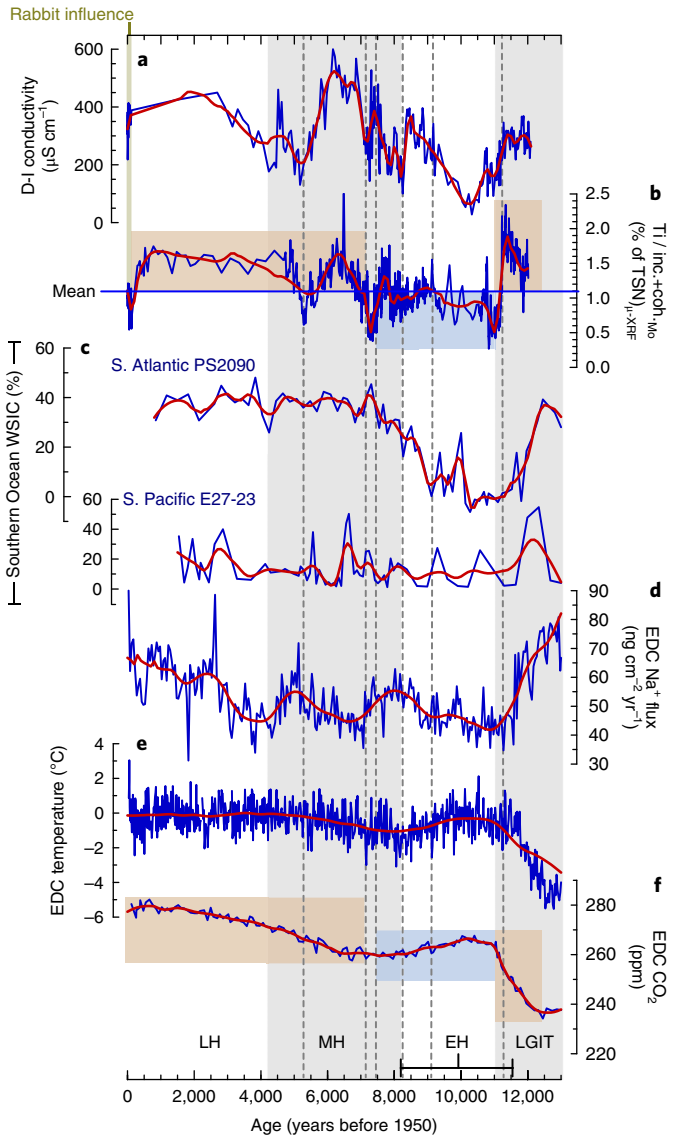

Fig. 3 | Comparison of Macquarie Island wind proxies with sea ice, temperature and CO_2. a, D-I conductivity. **b**, Titanium μ-XRF analysis. **c**, Southern Ocean WSIC from marine cores PS2090[29] and E27-23[30]. **d**, EPICA Dome C ssNa aerosol flux (representing new sea ice surfaces)[38]. **e**, EPICA Dome C temperature anomaly[32]. **f**, EPICA Dome C CO_2 (ref. [39]). Abbreviations as in Fig. 2. Grey dashed lines are lithological zones defined in Fig. 2. Orange shading highlights periods when above-mean winds correspond to increasing CO_2, blue shading when below-mean winds correspond to decreasing CO_2.

east and south of New Zealand[34]. If replicated in further studies, this would suggest a widespread decrease in wind intensity across the Southern Hemisphere from 41° S to 54° S (Macquarie Island; see Supplementary Note 7). The sustained warm conditions and low wind intensity during this period corresponded with reduced sea ice in marine[27,29] and ice-core records[35], and was followed by the only long-term decline in atmospheric CO_2 (about 10.5–7.2 ka) since the Antarctic Cold Reversal[36].

9.2–5.3 ka. All three wind proxies at Emerald Lake show a period of increased and higher-amplitude changes in wind intensity (relative to the early Holocene Thermal Maximum), punctuated by relatively short-lived (multi-centennial) periods when wind strength is significantly lower. This corresponds to some terrestrial records of enhanced precipitation in South America (for example at Tamar Lake[32] and Lago Cipreses[33], but not others[8]; see Supplementary Note 7). These increased winds coincide with a downturn in temperature and increases in sea ice (Fig. 3c,d). During the first part of this period, the positive relationship between enhanced winds and sea ice appears similar to the beginning of the record (12.1–11.2 ka), but differs, at least until 7 ka, because the winds did not correspond with an increase in atmospheric CO_2 (Fig. 3f). We attribute this to the concurrent development of alternative carbon sinks in the terrestrial biosphere, including mineral soils, peat and permafrost carbon[37,38]. However, after 7 ka, increased wind strength and sea ice correspond to the onset of the steady increase in atmospheric CO_2 that characterized the middle and late Holocene.

5.3–0 ka. This period of relatively constant and intense winds at Macquarie Island and elevated rainfall inferred from several studies on the western side of the Andes (see Supplementary Note 7, Supplementary Fig 15) corresponds with: relatively high sea ice in the Atlantic sector (Fig. 3c); increases in the ice-core ssNa after 4 ka (Fig. 3d); and a sustained increase in atmospheric CO_2 (Fig. 3f). Combined, this evidence implies that persistent strong winds led to net Southern Ocean outgassing during the latter part of the Holocene. Over the past 0.2 kyr, our record of Ti aerosol inputs into Emerald Lake shows an initial decline, followed by an increase in about the past 100 years. The latter is consistent with instrumental records from Macquarie Island, and other areas of the Southern Ocean, which have shown an intensification and southward shift in the main wind belt[5] (Supplementary Fig. 2). However, during this period, all proxies are potentially compromised by erosional inputs associated with the activities of introduced species[39] ('rabbit influence'; Fig. 2).

SHW, CO_2, temperature and sea ice

To develop our understanding of Southern Hemisphere climate dynamics, we now focus on the centennial to millennial relationships between the SHW, atmospheric CO_2, temperature and sea ice, and the extent to which they are replicated in selected global climate models.

First, the Macquarie record shows significant positive relationships between SHW and sea ice particularly through the late LGIT and early Holocene, and possibly during the period of sustained relatively intense winds from 5.3 to 0.2 ka (Supplementary Table 4, Supplementary Note 5). This is consistent with models from the Coupled Model Intercomparison Project Phase 5 (CMIP5) that show significant relationships between SHW jet strength and sea ice area[40]. It has been suggested that a strengthened SHW jet leads to increased Ekman upwelling, bringing cooler subsurface water to the surface, and strengthened equatorward transport, which is conducive to increased sea ice[12]. Alternatively, at least part of the correspondence between the SHW reconstruction and ice-core ssNA could be attributed to direct wind-driven transport of ssNa to the Dome C ice-core site, independent of changes in sea ice extent, although this has previously been questioned based on chemical signatures in the ice[41]. Thus, except for the period 9.2–7 ka, for which the relationship is less clear, the Macquarie Island record suggests that, at centennial to millennial timescales during the Holocene, sea ice and the intensity of the SHW were broadly in phase.

Second, in terms of the relationship between the SHW and atmospheric temperature and CO_2, the Macquarie Island proxy records show that windier periods (those greater than the 95% upper bound of their long-term mean) correspond with periods of increasing atmospheric CO_2 (orange shading in Fig. 3b, f) from 12.1 to 11.2 ka, and in the past 7 kyr. Conversely, the period of lower than mean winds from 11.2 ka corresponds with decreasing atmospheric CO_2 (blue shading in Fig. 3b, f), and a downturn in temperature (Fig. 3e),

which persisted until about 8 ka. This relationship is reproduced in short-term CMIP5 model experiments, which consistently show a poleward shift and strengthening of the SHW jet in response to increasing greenhouse gases and stratospheric ozone[42]. These observations are consistent with enhanced wind-driven upwelling of CO_2 rich deep ocean waters, accounting for at least part of the increase in atmospheric CO_2 across the LGIT and into the early Holocene[3] and the past 7 ka, while periods of reduced wind strength enhance the Southern Ocean CO_2 sink. The greater magnitude of the increase in CO_2 during the late LGIT and early Holocene (Fig. 3) can be attributed to the higher CO_2 available for release from the glacial deep ocean[43]. In contrast, the moderate increases in CO_2 since 7 ka can be attributed to less CO_2 available for release from the ocean, and to the development of terrestrial carbon sinks[37].

SHW and the future of the Southern Ocean carbon sink

Our new records of the SHW, which are aligned with the core jets of the present-day Antarctic Circumpolar Current, suggest large changes in wind intensity over the past 12.1 kyr. This is in marked contrast to model simulations of the SHW across the Last Glacial Termination and Holocene, which simulate only relatively small wind speed anomalies ($\pm 1\,m\,s^{-1}$)[9,23,44,45]. The correspondence between strong and persistent SHW and the rise in CO_2 during the latter part of the LGIT into the early Holocene, and from 7 ka, suggests that the winds have contributed to the long-term outgassing of CO_2 from the ocean during these periods. This provides a longer-term perspective on the 30-year instrumental record of Δp_{CO_2} and SHW strength, which has been used to evaluate short-term changes in the behaviour of the Southern Ocean carbon sink[4,5]. Specifically, the palaeodata support the Le Quéré model[4], which suggests a wind-driven weakening of the Southern Ocean carbon sink (enhanced outgassing) before 2007 CE as the dominant process. It does not support the alternative Landschützer model[5], which proposes that a stabilization of the surface waters has counteracted the wind-induced upwelling and reinvigorated the carbon sink during the past decade. Therefore, over multidecadal to millennial timescales, further increases in wind strength will lead to faster accumulation of CO_2 in the atmosphere.

Methods

Methods, including statements of data availability and any associated accession codes and references, are available at https://doi.org/10.1038/s41561-018-0186-5.

Received: 2 December 2017; Accepted: 19 June 2018;
Published online: 23 July 2018

References

1. Mikaloff-Fletcher, S. E. An increasing carbon sink?. *Science* **349**, 1165 (2015).
2. Hodgson, D. A. & Sime, L. C. Southern westerlies and CO_2. *Nat. Geosci.* **3**, 666–667 (2010).
3. Toggweiler, J. R., Russell, J. L. & Carson, S. R. Midlatitude westerlies, atmospheric CO_2, and climate change during the ice ages. *Palaeoceanography* **21**, PA2005 (2006).
4. Le Quéré, C. et al. Saturation of the Southern Ocean CO_2 sink due to recent climate change. *Science* **316**, 1735–1738 (2007).
5. Landschützer, P. et al. The reinvigoration of the Southern Ocean carbon sink. *Science* **349**, 1221–1224 (2015).
6. Munro, D. R. et al. Recent evidence for a strengthening CO sink in the Southern Ocean from carbonatesystem measurements in the Drake Passage (2002–2015). *Geophys. Res. Lett.* **42**, 2015GL065194 (2015).
7. Ritter, R. et al. Observation-based trends of the Southern Ocean carbon sink. *Geophys. Res. Lett.* **44**, 12339–12348 (2017).
8. Lamy, F. et al. Holocene changes in the position and intensity of the Southern Westerly wind belt. *Nat. Geosci.* **3**, 695–699 (2010).
9. Sime, L. C. et al. Southern Hemisphere westerly wind changes during the Last Glacial Maximum: model–data comparison. *Quat. Sci. Rev.* **64**, 104–120 (2013).
10. Anderson, R. F. et al. Wind-driven upwelling in the Southern Ocean and the deglacial rise in atmospheric CO_2. *Science* **323**, 1443–1448 (2009).
11. Lovenduski, N. S., Gruber, N. & Doney, S. C. Toward a mechanistic understanding of the decadal trends inthe Southern Ocean carbon sink. *Glob. Biogeochem. Cycles* **22**, GB3016 (2008).
12. Purich, A., Cai, W., England, M. H. & Cowan, T. Evidence for link between modelled trends in Antarctic sea ice and underestimated westerly wind changes. *Nat. Commun.* **7**, 10409 (2016).
13. Wanninkhof, R. et al. Global ocean carbon uptake: magnitude, variability and trends. *Biogeosciences* **10**, 1983–2000 (2013).
14. Kilian, R. & Lamy, F. A review of Glacial and Holocene paleoclimate records from southernmost Patagonia (49–55°S). *Quat. Sci. Rev.* **53**, 1–23 (2012).
15. Fontana, S. L. & Bennett, K. Postglacial vegetation dynamics of western Tierra del Fuego. *Holocene* **22**, 1337–1350, (2012).
16. Waldmann, N. et al. Integrated reconstruction of Holocene millennial-scale environmental changes in Tierra del Fuego, southernmost South America. *Palaeogeogr. Palaeoclimatol. Palaeoecol.* **399**, 294–309 (2014).
17. Moy, C. M. et al. Isotopic evidence for hydrologic change related to the westerlies in SW Patagonia, Chile during the last millennium. *Quat. Sci. Rev.* **27**, 1335–1349 (2008).
18. Bertrand, S., Hughen, K., Sepúlveda, J. & Pantoja, J. Late Holocene covariability of the southern westerlies and sea surface temperature in Northern Chilean Patagonia. *Quat. Sci. Rev.* **105**, 195–208 (2014).
19. Lamy, F. et al. Antarctic timing of surface water changes off Chile and Patagonian ice sheet response. *Science* **304**, 1959–1962 (2004).
20. Strother, S. L. et al. Changes in Holocene vegetation, climate and the intensity of Southern Hemisphere Westerly Winds based on a high-resolution palynological record from sub-Antarctic South Georgia. *Holocene* **25**, 263–279 (2015).
21. Turney, C. S. M. et al. A 250-year periodicity in Southern Hemisphere westerly winds over the last 2600 years. *Clim. Past* **12**, 189–200 (2016).
22. Vanneste, H. et al. Late-glacial elevated dust deposition linked to westerly wind shifts in southern South America. *Sci. Rep.* **5**, 11670 (2015).
23. Sime, L. C. et al. Sea ice led to poleward-shifted winds at the Last Glacial Maximum: the influence of state dependency on CMIP5 and PMIP3 models. *Clim. Past* **12**, 2241–2253 (2016).
24. *Climate Statistics for Australian Locations, Macquarie Island* (Australian Government Bureau of Meterology, 2017); http://www.bom.gov.au/climate/averages/tables/cw_300004_All.shtml
25. Saunders, K. M., Hodgson, D. A. & McMinn, A. Quantitative relationships between benthic diatom assemblages and water chemistry in Macquarie Island lakes and their potential to reconstruct past environmental changes. *Antarct. Sci.* **21**, 35–49 (2009).
26. Röthlisberger, R. et al. Dust and sea salt variability in central East Antarctica (Dome C) over the last 45 kyrs and its implications for southern high-latitude climate. *Geophys. Res. Lett.* **29**, 24-1–24-4 (2002).
27. Xiao, W., Esper, O. & Gersonde, R. Last Glacial-Holocene climate variability in the Atlantic sector of the Southern Ocean. *Quat. Sci. Rev.* **135**, 115–137 (2016).
28. Ferry, A. J. et al. First records of winter sea ice concentration in the southwest Pacific sector of the Southern Ocean. *Paleoceanography* **30**, 1525–1539 (2015).
29. Bianchi, C. & Gersonde, R. Climate evolution at the last deglaciation: the role of the Southern Ocean. *Earth Planet. Sci. Lett.* **228**, 407–424 (2004).
30. Jouzel, J. et al. Orbital and millennial Antarctic climate variability over the past 800,000 years. *Science* **317**, 793–796 (2007).
31. Masson, V. et al. Holocene climate variability in Antarctica based on 11 ice-core isotope records. *Quat. Res.* **54**, 348–358 (2000).
32. Fletcher, M.-S., & Moreno, P. I. Zonally symmetric changes in the strength and position of the Southern Westerlies drove atmospheric CO_2 variations over the past 14 k.y. *Geology* **39**, 419–422 (2011).
33. Moreno, P. I. et al. Onset and evolution of southern annular mode-like changes at centennial timescale. *Sci. Rep.* **8**, 3458 (2018).
34. Prebble, J. G. et al. Evidence for a Holocene Climatic Optimum in the southwest Pacific: a multiproxy study. *Paleoceanography* **32**, 763–779 (2017).
35. Röthlisberger, R. et al. *EPICA Dome C Ice Core nss-Ca and Na Data. IGBP PAGES/World Data Center for Paleoclimatology Data Contribution Series #2005-046* (NOAA/NGDC Paleoclimatology Program, 2005).
36. Monnin, E. et al. Atmospheric CO_2 concentrations over the Last Glacial Termination. *Science* **291**, 112–114 (2001).
37. Brovkin, V. et al. Comparative carbon cycle dynamics of the present and last interglacial.*Quat. Sci. Rev.* **137**, 15–32 (2016).
38. Stocker, B. D., Yu, Z., Massa, C. & Joos, F. Holocene peatland and ice-core data constraints on the timing and magnitude of CO2 emissions from past land use. *Proc. Natl Acad. Sci. USA* **114**, 1492–1497 (2017).
39. Saunders, K. M. et al. Ecosystem impacts of feral rabbits on World Heritage sub-Antarctic Macquarie Island: a palaeoecological perspective. *Anthropocene* **3**, 1–8 (2013).
40. Bracegirdle, T. J., Hyder, P. & Holmes, C. R. CMIP5 diversity in southern westerly jet projections related to historical sea ice area: Strong link to strengthening and weak link to shift. *J. Clim.* **31**, 195–211 (2018).

41. Wolff, E. W. et al. Southern Ocean sea-ice extent, productivity and iron flux over the past eight glacial cycles. *Nature* **440**, 491–496 (2006).
42. Bracegirdle, T. J. et al. Assessment of surface winds over the Atlantic, Indian, and Pacific Ocean sectors of the Southern Ocean in CMIP5 models: historical bias, forcing response, and state dependence. *J. Geophys. Res. Atmos.* **118**, 547–562 (2013).
43. Köhler, P., Fischer, H., Munhoven, G. & Zeebe, R. E. Quantitative interpretation of atmospheric carbon records over the last glacial termination. *Glob. Biogeochem. Cycles* **19**, GB4020 (2005).
44. Chavaillaz, Y., Codron, F. & Kageyama, M. Southern westerlies in LGM and future (RCP4.5) climates. *Clim. Past* **9**, 517–524 (2013).
45. Rojas, M. Sensitivity of Southern Hemisphere circulation to LGM and $4\times CO_2$ climates. *Geophys. Res. Lett.* **40**, 965–970, (2013).

Acknowledgements

This research was funded by NERC Standard grant NE/K004514/1 (D.A.H., S.J.R., L.S.), Swiss National Science Foundation Ambizione Postdoctoral Research Fellowship PZ00P2_136835/1 (K.M.S.), Swiss National Science Foundation Grant 200021_172586 (M.G.) and Australian Antarctic Science grants 3117 and 4156 (K.M.S.). K.M.S. was also supported by PhD funding as part of grant 2663 to A. McMinn, an Australian Postgraduate Award (2004–2008) and an Australian Institute of Nuclear Science and Engineering Postgraduate Research Award. The Australian Antarctic Division and the Parks and Wildlife Service Tasmania provided logistical support and access to the Macquarie Island World Heritage Area. Field support was provided by A. O'Hern, A. Wakefield, C. Oosthuizen, B. Arthur, J. van Dorst, J. Pitcher, S. Williams, T. Blyth and Parks and Wildlife Service Rangers and volunteers. We thank H. Lu of the British Antarctic Survey for providing and adapting MATLAB scripts for sequential Mann-Kendall test analyses, A. Whittle for processing the wind data and underlying geotifs in Fig. 1a and b, and D. Fischer, S. Arcusa and N. Tunstall for technical support.

Author contributions

D.A.H., K.M.S. and S.J.R. contributed equally to this work. Fieldwork was carried out by K.M.S., D.A.H., S.J.R. and W.V.N. Analytical work was performed by S.J.R. (μ-XRF, sedimentology, chronology and statistical analyses) and S.D. (μ-XRF), K.M.S. and B.P. (D-I conductivity analyses, chronology and sedimentology), W.V.N. (fieldwork and diatom analysis), K.M.S., C.B. and M.G. (hyperspectral imaging) and L.S. (modelling). D.A.H., K.M.S., S.J.R. and B.P. wrote the manuscript and Supplementary Information with input from all authors.

Competing interests

The authors declare no competing interests.

Additional information

Supplementary information is available for this paper at https://doi.org/10.1038/s41561-018-0186-5.

Correspondence and requests for materials should be addressed to K.M.S.

Methods

A series of lake sediment cores dating back to about 12.1 ka was extracted from Emerald Lake on the western edge of the Macquarie Island plateau. Perched within a small catchment, Emerald Lake is ideally situated to record changes in sea-salt and mineral aerosol inputs (Supplementary Notes 2, 3). We applied three independent methods to reconstruct past changes in SHW intensity (Supplementary Note 5). First, to reconstruct past sea-salt aerosol inputs, we developed a method to track past changes in lake water conductivity (a function of sea-salt aerosol input) using diatom-based inference models[25,46]. These use the strong statistical relationship between modern diatom species assemblages and lake water conductivity (weighted averaging partial least squares, two components; $r^2 = 0.92$, $r^2_{jackknife} = 0.72$, root-mean-square error of prediction (RMSEP) = 230 µS cm^{-1}; Supplementary Note 5), which is applied as a transfer function to reconstruct past changes in conductivity from subfossil species assemblages preserved in lake sediments. Second, data from an Itrax µ-XRF Core scanner were used to track inputs of minerogenic aerosols into the lake, focusing on titanium, one of the most widely used indicator elements for increased allochthonous inputs[47] from distal and proximal sources[48]. Third, cores were scanned using a Specim hyperspectral camera, which measures reflected optical properties between wavelengths from 400 to 1,000 nm (ref. [49]). The ratio of reflectance between 850 nm and 900 nm (R_{850}/R_{900}) was used as an additional indicator of minerogenic inputs. Statistical analyses of the proxies were undertaken using R version 2.15.2 (R Foundation for Statistical Computing), MATLAB (see Supplementary Note 3 for details) and Sigmaplot v13, using original and 100-year-interval second-order polynomial LOESS (local tricube weighting and polynomial regression) smoothing. The calibration and performance of each of these methods together with details of core sedimentology and chronology are described in Supplementary Notes 3, 4 and 5. Potential influences on the proxies (such as lake ice cover and relative sea level) are described in Supplementary Note 6.

Data availability. All data are archived at the Australian Antarctic Data Centre (https://data.aad.gov.au/) and Natural Environment Research Council Polar Data Centre (https://www.bas.ac.uk/data/uk-pdc/).

References

46. Van Nieuwenhuyze, W. *Reconstruction of Holocene Paleoenvironmental Changes in the Sub-Antarctic Region.* PhD thesis, Univ. Ghent (2015).
47. Davies, S. J., Lamb, H. F. & Roberts, S. J. in *Micro-XRF Studies of Sediment Cores* (eds Croudace I. W. & Rothwell R. G.) 189–226 (Springer, Dordrecht, 2015).
48. Heimburger, A., Losno, R., Triquet, S. & Nguyen, E. B. Atmospheric deposition fluxes of 26 elements over the Southern Indian Ocean: time series on Kerguelen and Crozet Islands. *Glob. Biogeochem. Cycles* **27**, 440–449 (2013).
49. Butz, C. et al. Hyperspectral imaging spectroscopy: a promising method for the biogeochemical analysis of lake sediments. *J. Appl. Remote Sens.* **9**, 096031 (2015).